Transport Studies Using Laser Blow-Off injection of Low-Z Trace Impurities Injected into the TJ-II Stellarator

B. Zurro 1), E. Hollmann 2), M. Tillack 2), C. Clark 3), A. Baciero 1), M. A. Ochando 1), F. Medina 1), K. J. McCarthy 1), E. Blanco 1), E. de la Cal 1), D. Carralero 1), M. A. Pedrosa 1) and TJ-II team 1)

1) Laboratorio Nacional de Fusión, Asociación EURATOM-CIEMAT, Madrid, Spain
2) University of California, San Diego, La Jolla, U.S.A.
3) University of Wisconsin, Madison, U.S.A.

E-mail contact of main author: b.zurro@ciemat.es

Abstract. Laser blow-off of low-Z (boron and carbon) material is used to study parallel and radial impurity ion transport, as well as radial heat transport, in the TJ-II stellarator. Toroidal transport is found to be, consistent with entrainment in edge toroidal rotation. Radial/poloidal transport and loss to the plasma edge is seen to be slower (about 5 ms) and is clearly seen to be slower for carbon than for boron, consistent with collisional (neoclassical) cross-field transport. Radial heat transport is observed to be quite rapid (0.1 ms time scale).

1. Introduction

The simultaneous achievement of high energy and low impurity confinement times is crucial for achieving fusion plasmas. A critical issue in stellarators is the avoidance of impurity accumulation [1]. Previous studies of impurity confinement in electron cyclotron resonance heated (ECRH) plasmas in the TJ-II stellarator [2-4] have focused on heavy (iron) impurities. Moderate (~ 10 ms) confinement times were observed at low densities when the radial electric field, E_r, in the plasma core was positive. However, when close to or above the density value where the transition to negative E_r occurs, a significant rise in impurity confinement time (to ~20 ms) was observed, in particular with neutral beam injection (NBI) heating [4]. In this paper, transport of light (boron and carbon) impurities in TJ-II ECRH plasmas with a fresh lithium wall coating is studied [5]. Laser blow-off injection (LBI) is used to create an impurity deposition which is very localized spatially, allowing the study of both toroidally and radial impurity ion propagation. Also, the simultaneous injection of both boron and carbon allows the transport properties of the two impurity species can be compared simultaneously. Overall, the experiments observe a very rapid (~0.5 ms) toroidal impurity transport followed by a slower (~5 ms) radial/poloidal impurity loss to the chamber walls. The toroidal impurity transport is consistent with entrainment in the (~1 kHz) edge toroidal plasma rotation. The radial impurity loss is observed to be slower for carbon than for boron ions, qualitatively consistent with collisional (neo-classical) transport.

In addition to impurity transport, preliminary measurements of heat transport of the LBI cold pulse are presented. The study of cold pulse propagation, using either laser blow-off or pellet injection, has shown that electron energy transport has a localized character in the W7-AS stellarator [6] and the RFP reversed-pinch [7], which is in contrast to the LHD stellarator [8] and to tokamaks such as TEXT [9] and JET [10] which exhibit non-local behaviours. In the TJ-II cold pulse propagation was previously studied using nitrogen puffing [11]. Here, a method is described to determine the delay and decay times of the perturbation detected by an Electron Cyclotron Emission (ECE) radiometer [12] for a range of plasma densities.

The paper is organized as follows: first, an overview of the experiment is given; next, the confinement time of impurities in ECRH discharges, when measurable, is studied as a

function of density. Second, the parallel transport of B and C is studied in a similar scan. Finally, electron temperature perturbations are analysed for a selected set of discharges.

2. Experimental Set-up

TJ-II is a four-period, low magnetic shear stellarator with major and averaged minor radii of 1.5 m and $\leq$0.22 m, respectively. Central electron densities and temperatures up to 1.7×10^{19} m^{-3} and 1 keV respectively are achieved for plasmas created and maintained by ECRH at the second harmonic (f = 53.2 GHz, $P_{ECRH} \leq$ 400 kW). LBI was performed with two different trace impurities: boron and boron-carbide (B_4C). In each case the material was deposited as a 2 μm thick film on a glass sample. The first, a boron sample with a thin (10 nm) top film of Cr, was provided by (LeBow, Goleta, CA) while the second sample (B_4C), was deposited at the UC San Diego using a magnetron. For blow-off, a Q-switched Nd-YAG laser (800 mJ, 10 ns), focussed to a 1 mm diameter spot, was used. The LBI system is described in Ref. [2].

In the experiment, the trace impurities (providing <5% of the initial total electron number) are injected at ϕ = 0º of FIG. 1(a). The initial rapid parallel transport of the resultant ions is measured using filterscopes set to monitor B II and C III emission lines and located on opposite sides of the torus, see FIG. 1(a). For this, two filterscopes are located near the laser blow-off sector while another two view a poloidal limiter on the opposite side of the machine, *i.e.*, at ϕ = 180º.
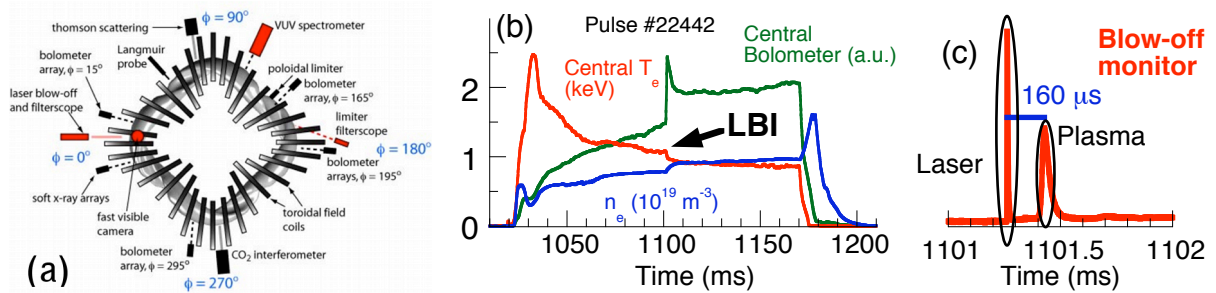

FIG. 1. (a) A top view of TJ-II showing diagnostic and laser blow-off locations; (b) Radiated power (bolometer signal), electron temperature (ECE channel) and electron density (interferometer) during an injection discharge; (c) Expanded blow-off monitor signal where the first peak establishes the laser shot time while the second peak marks the interaction time of the ablated particles with the plasma edge.

In FIG. 1(b), we show signals for a TJ-II discharge into which boron is injected. Responses to the injection of central viewing bolometer, as well as of ECE monitor at similar radial position. Finally, FIG. 1(c) elucidates how impurity velocity is determined from the time lapse between signals from the laser shot and the arrival of the plume at the plasma edge.

3. Results and Discussion

3.1. Global Confinement

Results of confinement times are depicted in FIG. 2 for B-Cr and B-C injected into a series of similar ECRH discharges. For this, confinement times were estimated from the decay of the perturbation signals in the global radiation monitors. The most notable result is the clear difference in confinement values for the different samples. This is seen in the plot of averaged values (a), where data from several monitors are shown, and in the plot of perturbation decay

determined from the C V signal (b). A similar trend, though not shown here, is observed with integrated or locally inverted bolometric data. It should be noted that the experiments were performed shortly after a new lithium coating was deposited on the TJ-II wall, the effect being more notable for B-C when plasma discharges were cleaner, (see FIG. 2(c) where the radiation level divided by density, a qualitative measurement of Z_{eff}, is significantly reduced for this case). Finally, the localized reconstruction of the perturbation using data from a bolometric array allows deduction of the decay time dependence on reduced radius, see FIG. 2(d).
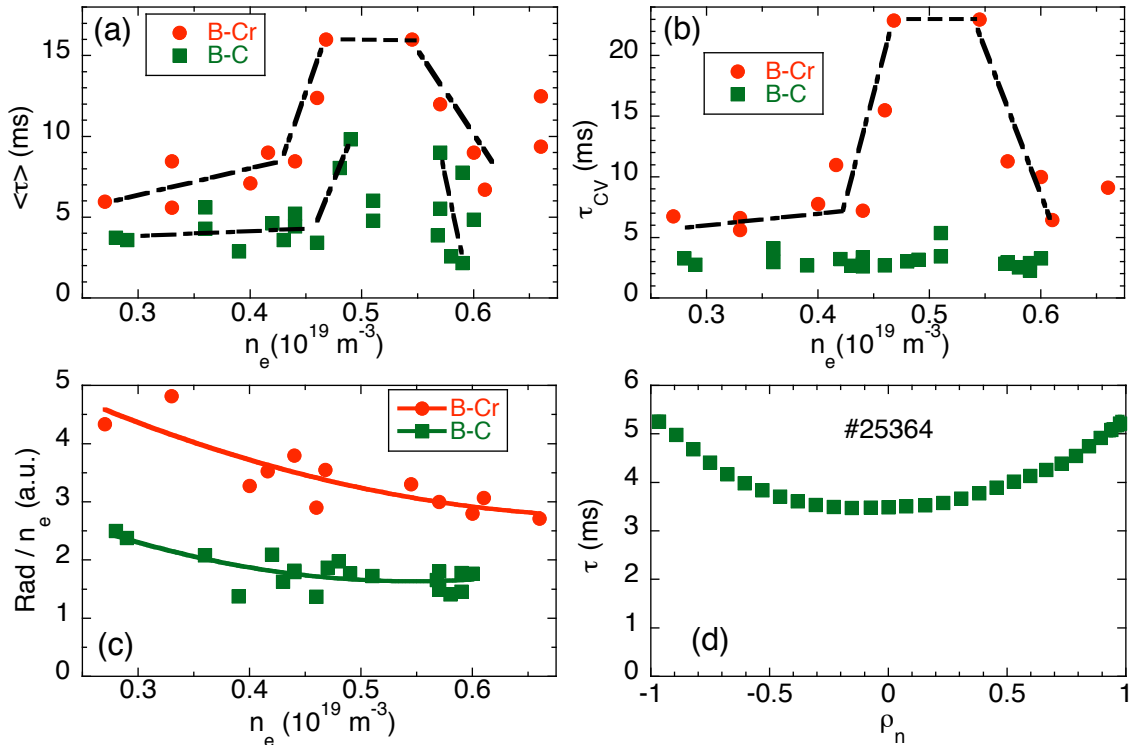

FIG. 2. A comparison of light-impurity confinement times versus density for two sequences of discharges: (a) Averaged confinement time when injecting for B-Cr (full red points) and B-C (green squares) samples; (b) Confinement times deduced from C V spectral line monitor for same experiment; c) Plot of contamination of both sequences quantified by the ratio of global radiation divided by density; (d) Local behaviour of perturbation decay time as deduced from local bolometric reconstruction.

These data show a tendency for increasing confinement with increasing electron density up to a density value of around 0.5 where the confinement starts to decrease as we move toward higher densities close to the point where the transition from positive E_r to negative takes place [13]. This high-density region was inaccessible in previous experiments in TJ-II that were performed without a lithium wall coating [2]. In contrast to tokamaks, all thermodynamic forces in stellarators are predicted to support core impurity accumulation in the standard case with negative E_r, the so-called ion-root regime [1].

3.2. Parallel Transport

Fast visible camera images of the injection region were recorded, with an intensifier, at 100 kHz with a B II (412 nm) filter. For this the view was vertical downwards on the blow-off/plasma interaction region, see FIG. 1. In this way, impurity deposition in the plasma was found to be quite localized to the injection region as well as in time (for a pulse of length 0.1

– 0.2 ms). Typically, material interacting with the plasma edge appears to form an amorphous mist or dust cloud, see FIG. 3 and FIG. 4. However for one shot (#25355) a single large boron pellet was produced, this being interesting as the pellet appeared to be transported radially past the plasma edge. Evidence for a rapid (Mach number $M > 1$) counter-clockwise toroidal flow was seen in the toroidally asymmetric pellet ablation plume, which is consistent with previous toroidal rotation measurements of peripheral ions of about 1 kHz [14].
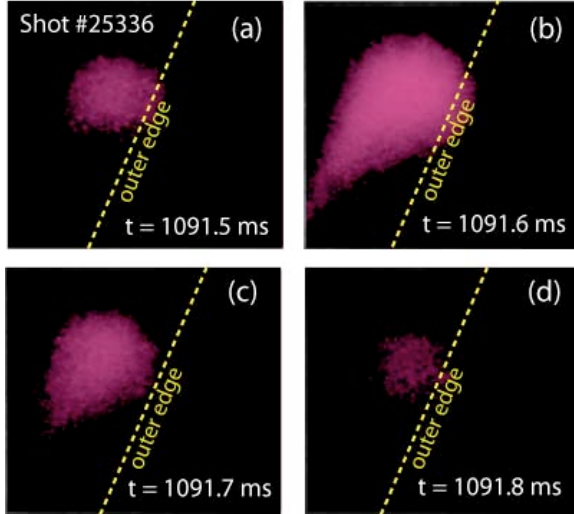

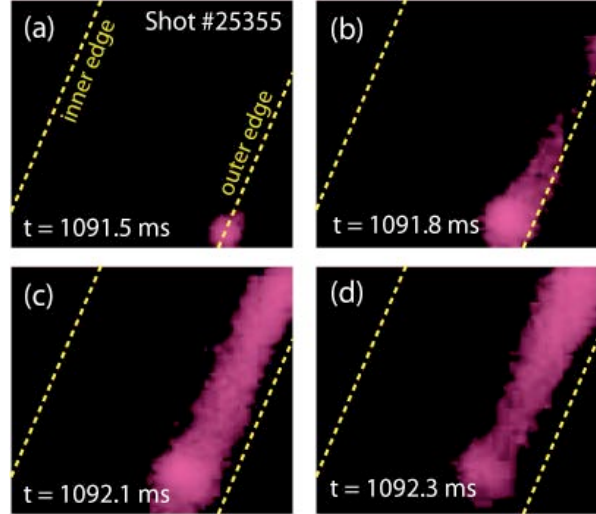FIG. 3. B II (412 nm) images of ablated boron interaction with the plasma edge (shot #25336).

FIG. 4. B II (412 nm) images of ablated boron interaction with the plasma edge in which a single large boron pellet occurs (shot #25355).

In addition, clear delays are seen between the filterscope signals at the blow-off location and at the limiter at $\phi = 180º$, see FIG. 5 where time traces of B II (345 nm) and C III (465 nm) line intensities are shown. Note: absolute calibrations were performed subsequently using a calibration sphere. The injection pulse in FIG. 5 can be seen to be quite narrow compared with the limiter recycling pulses.
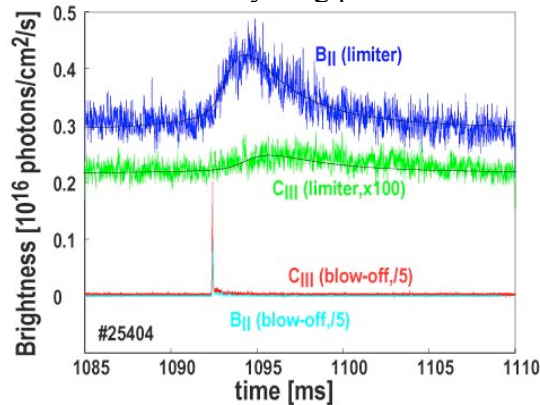

FIG. 5. Filterscope data showing time traces line intensities of B II (345 nm) at limiter, B II (412 nm) at injection location, and C III (465 nm) at both locations. Note that timing is off by ~ 1 ms in this figure (needs to be corrected for digitizer delay).
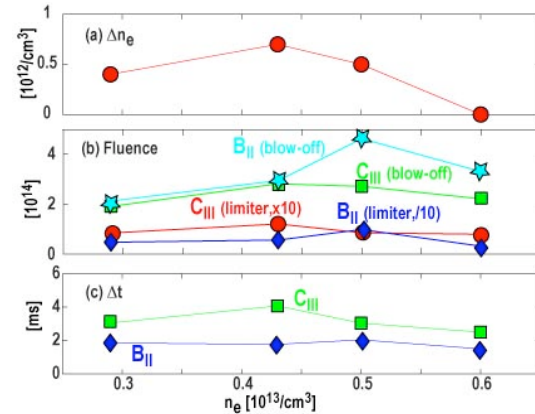
FIG. 6. Perturbations versus target plasma density showing (a) line-integrated density perturbation Δn_e measured with an interferometer; (b) integrated particle fluence calculated from filterscope brightness (in units of total particle number); (c) delay in filterscope signal perturbation between injection and limiter locations.

Furthermore, the peak electron density perturbation, measured with an interferometer, is also shown in FIG. 6. For this experiment, the sample thickness was 2.1 μm of B_4C and the blow-

off spot was 1 mm in diameter. This corresponds to about 3.6×10^{16} boron and 9×10^{15} carbon atoms, respectively.   Since the plasma volume is ~ 1.2 m^3, these atoms, if fully assimilated and fully stripped, would cause an electron density perturbation, Δn_e, of $\sim 2 \times 10^{11}$ cm^{-3}, a value which is roughly consistent with the observed Δn_e of 2 - 6 x 10^{11} cm^{-3}.

Also plotted in FIG. 6 is the total integrated impurity fluence estimated from the filterscope signals having determined the absolutely-calibrated filterscope response plus ADAS inverse photon efficiencies (S/XB ratios) for the boron and carbon lines. For this, emissions were assumed to come from plasma with an electron temperature equal to half the corresponding ionization energy. However, total fluences estimated in this way appear very low, for example $\sim 2 \times 10^{14}$ carbon atoms in the injection region. To explain this it is possible that the filterscope observation volume is missing a significant fraction of the injected impurities. The recycling fluence of carbon measured at the limiter is very small, $\sim 10^{13}$ carbon atoms, whereas that of boron is fairly large, $\sim 10^{15}$ boron atoms, *i.e.* boron recycling off the limiter is x100 times that for carbon. The reason for this large discrepancy is not yet understood; the expected factor is x4. In contrast, the boron and carbon fluences at the injection location are roughly comparable, as would be expected.

Time delays of 2 ms for boron and 3 ms for carbon are observed between filterscope signals from the injection and limiter locations. These correspond to toroidal velocities (for a 4.5 m path length between the injection point and the limiter) of $\sim 2 \times 10^3$ and 1.5×10^3 m/s, respectively, which gives ion thermal velocities, T_i, of ≈ 0.3 - 0.4 eV. These T_i values appear too low to be realistic, so it is probable that the time delay is limited by transport (diffusion) processes, rather than direct parallel ion transit.
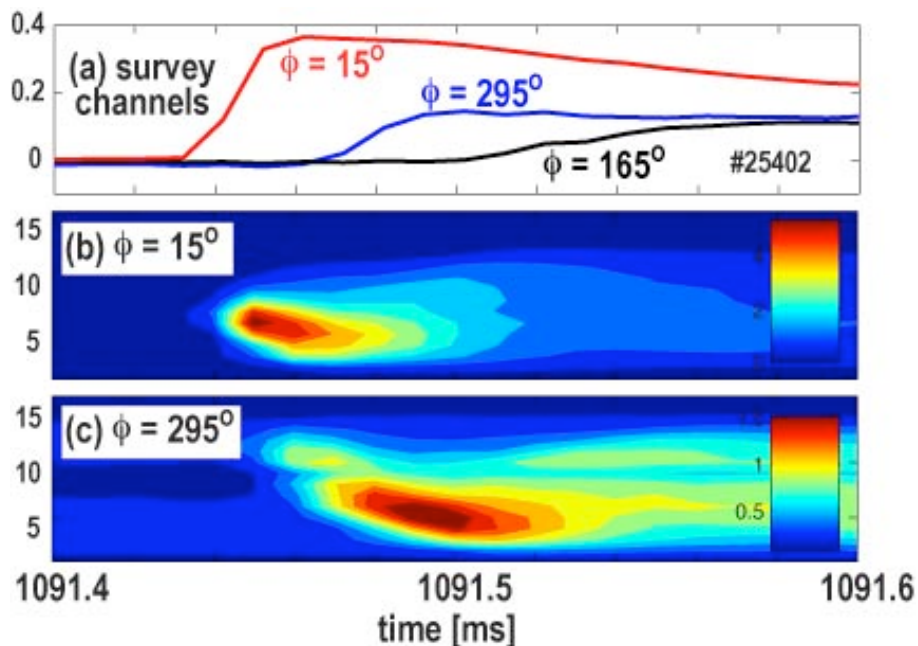

FIG. 7. AXUV bolometer data showing (a) survey channel data for several toroidal locations, plus poloidal array brightness contours for (b) $\phi = 15°$ and (c) $\phi = 295°$.

AXUV photodiode systems (fast bolometers) are located at several toroidal locations around TJ-II, see FIG. 1(a). These include several 16 channel, poloidally aligned, arrays as well as wide-angle photodiodes, which essentially integrate over the entire poloidal cross-section. In FIG. 7, a delay in arrival time of the radiating boron impurity is plotted for wide-angle

photodiodes at different toroidal locations is observed. Signal intensity contour plots for the 16 channels versus time are included in the same figure. From these, it is apparent the injected impurity (boron) is localized poloidally at the two positions highlighted although there is some evidence for poloidal transport/drift.
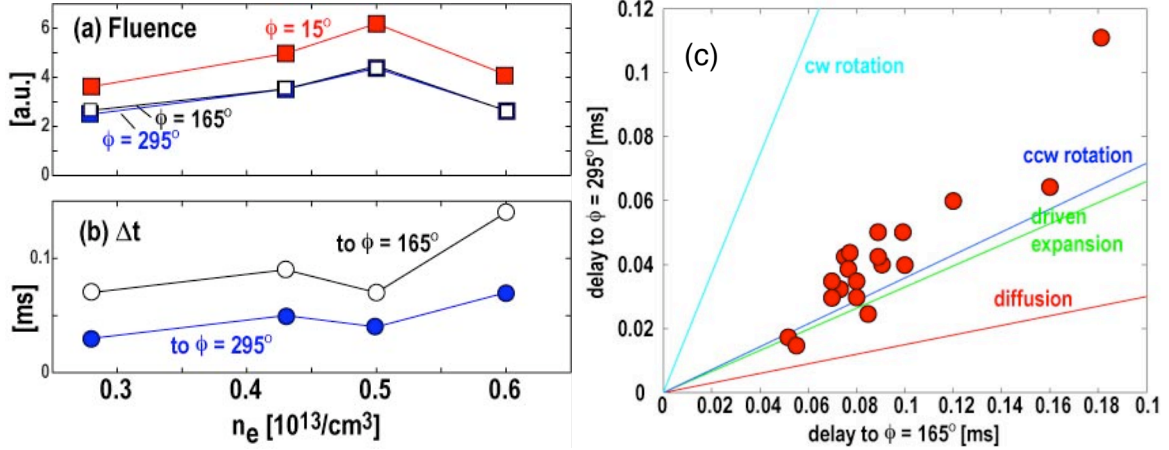

FIG. 8. Overview of AXUV bolometer data for a density scan: (a) Fluence (integrated brightness); (b) Delay time between signal brightness in injection region and 2 different toroidal locations; (c) Plot of delays between wide-angle bolometers to provide an overview of relative delays in core impurity transport.

Next, FIG. 8 provides an overview of bolometer data trends during a density scan showing fluence (brightness flash integrals in wide-angle channels) and time delays (time differences between "first light" at different toroidal locations). From this a clear correlation between fluences at the different locations on the machine and magnitudes is found thereby suggesting that there is no radial loss of impurities on this time scale, *i.e.* the impurity transiting the machine toroidally is semi-intact. This is supported by a clear correlation in the time delay data, i.e., the delays to the 1/4 and 1/2 positions around the machine ($\phi = 295°$ and $\phi = 165°$, respectively) differ by a factor of 2, this being consistent with a convective or kinetic (rather than diffusive) process. Also, the rapid toroidal transport time scales, of order 0.1 ms, suggest high boron ion temperatures, $T_i \sim 200$ eV. From the data here, it is not obvious if this rapid core ion transport is kinetic (collisionless), transit or entrainment in core toroidal rotation. At present, the observed trend appears to be more consistent with either impurity entrainment in a counter-clockwise rotating plasma or impurity expansion in both directions in a driven expansion (*e.g.*, by a pressure driven flow); see FIG. 8(c).

Further information was obtained using a VUV spectrometer equipped with a CCD camera operated with a 3.84 ms integration time. In FIG. 9, the emission lines observed in a 20 nm wide survey centered about 50 nm are identified. In contrast, in surveys centered about 120 and 150 nm only the weak H I line (121.57 nm) and C IV lines (154.8 and 155.1 nm) were distinguished. Moreover, although the time resolution is poor, temporal traces of observed carbon and boron lines show that residence times of the carbon ions are slightly longer than those of the boron ions. However, no clear differences in residence times are seen between different charge states of the same species, e.g. boron. In addition, the signal ramp-up times are several ms, these being much slower than for the bolometers, so possibly the VUV spectrometer view chord misses the peak of the initial impurity pulse. Overall, the VUV spectrometer data is consistent with the filterscope data, i.e. with loss to the plasma walls on a 5-10 ms time scale with an increased time scale for carbon when compared with boron.
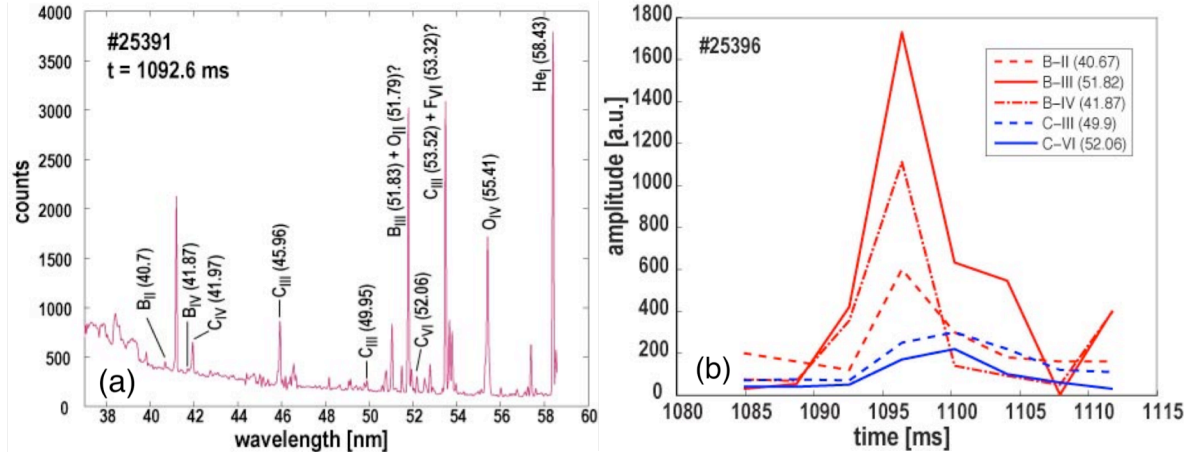
FIG. 9. (a) VUV spectrometer spectrum for boron-carbide injection with the strongest lines labeled; (b) Time evolution of the B and C lines found in the region following injection.

Finally, probe data were obtained at 2 MHz with a stationary, 12-radial pin probe, having 6 pins measuring J_{sat} and 6 measuring V_{float}. After analysis, only very small perturbations were seen after impurity injection in both signals, indicating that the impurity injection is not strongly perturbing the edge plasma profile or edge plasma turbulence.

3.3. Electron Temperature Perturbation

In addition to studying impurity transport, LBI creates a cold front which can be used to study cross-field heat transport. In order to track the temporal evolution of the cold-front time, signals from the blow-off monitor, at the injection port, and from the multi-channel heterodyne ECE radiometer were considered, the latter following the perturbation in electron temperature, T_e, at different radii with good temporal resolution. Then, in order to calculate the perturbation decay time for an ECE channel in the time window where the ECE signal is transiently perturbed, the temporal T_e evolution is fitted to:

$$T_e(t) \;=\; T_{e0} \;+\; H(t - t_0)(T_{e1} - T_{e0})\;(1 - e^{-t/\tau}) \tag{1}$$

where $H(t)$ is the Heaviside function. Here, T_{e0}, T_{e1}, t_0 and τ (decay time) are determined with a non-linear least squares fit. An example of the application of this method is given in FIG. 10(a). It should be noted that t_0 is good agreement for all 4 central channels (not shown), thus indicating that the perturbation is felt almost simultaneously by all central channels, *i.e.* there is no detected propagation. These results differ from those obtained in a previous study of the propagation of a transient perturbation in T_e produced by strong nitrogen puffing [10]. In that case, the edge ECE channels responded significantly faster than the central ones, with delays of $\approx$2 ms. This suggests that the underlying physics for the different methods is quite different, presumably because in the former case the T_e perturbation is introduced very rapidly in a toroidally localized region.

The exponential recovering time for a set of ECE channels has been studied in a sequence of discharges with different background electron density where B$_4$C was injected by laser blow-off. The averaged value, for a set of central ECE channels, is plotted in FIG. 10(b) versus density. The recovering time increases as the density increases, as expected due to the

improvement of the electron energy transport with density. Overall, cross-field heat transport time scales of order 100 µs are observed.
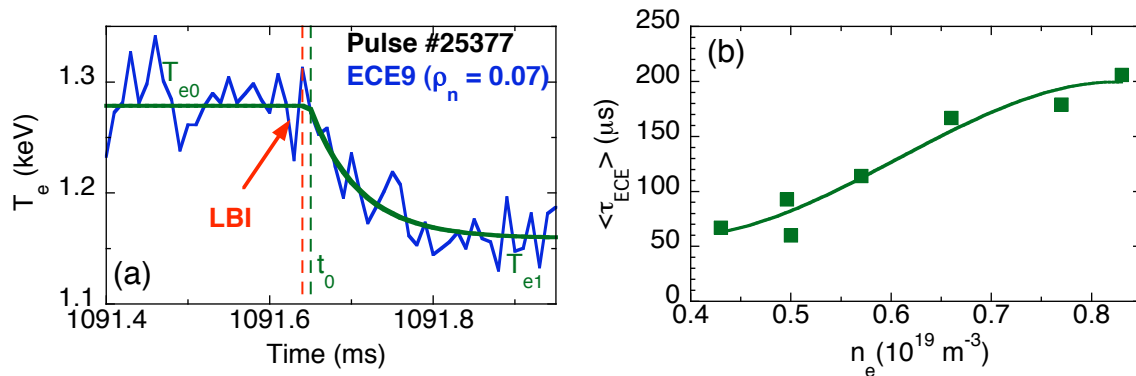

FIG. 10. (a) Analysis of one ECE channel in TJ-II discharge #22442. The perturbations is fitted by an exponential decay where blue is T_e measured with the ECE radiometer; the broken red line indicates the laser shot; the broken green line is t_0; and the solid line (green) is the fitted function; (b) Plot of the averaged exponential recovering time, for a set of ECE central channels, as a function of electron density.

References

[1] R. BURHENN et al., Nucl. Fusion **49** (2009) 065005.
[2] B. ZURRO et al., Proc. 20th IAEA Conference, Paper (2004) EX/P6-32.
[3] C. HIDALGO and TJ-II Team, Nucl. Fusion **45** (2005) S266.
[4] B. ZURRO, A. BACIERO, E. HOLLMANN et al., Proc. 36th EPS Conf. Plasma Phys. ECA **33E** (2009) P-4.191.
[5] F. L. TABARÉS et al., Plasma Phys. Control. Fusion **50** (2008) 124051.
[6] H. WALTER, U. STROTH, J. BLEUEL et al., Plasma Phys. Control. Fusion **40** (1998) 1661.
[7] L. FRASSINETTI, D. TERRANOVA, Y. HIRANO et al., Nucl. Fusion **47** (2007) 135.
[8] N. TAMURA, S. INAGAKI, K. TANAKA et al., Nucl. Fusion **47** (2007) 449.
[9] K.W. GENTLE, R.V. BRAVENEC, G. CIMA et al., Phys. Fluids **2** (1995) 2292.
[10] JET Team, Proc. 15th Int. Conf. on Plasma Physics and Controlled Fusion **1** (1995) 307.
[11] B.P van MILLIGEN, E. de la LUNA, F.L. TABARÉS et al., Nucl. Fusion **42** (2002) 787.
[12] E. de la LUNA, J. SÁNCHEZ, V. TRIBALDOS and T. ESTRADA, Rev. Sci. Instrum. **72** (2001) 379.
[13] B. ZURRO et al., Fusion Science and Technology **50** (2006) 419.
[14] D. RAPISARDA, Study of ion dynamics by spectroscopy methods in TJ-II, PhD Thesis, Univ. Complutense de Madrid (2006).